

Removable and/or Repeated Units Emerge in Overparametrized Deep Neural Networks

Stephen Casper^{*,1,5} Xavier Boix^{*,1,2,5}
Vanessa D’Amario³ Ling Guo⁴ Martin Schrimpf^{2,5} Kasper Vinken^{1,5} Gabriel Kreiman^{1,5}
scasper@college.harvard.edu, xboix@mit.edu

Abstract

Deep neural networks (DNNs) perform well on a variety of tasks despite the fact that most networks used in practice are vastly overparametrized and even capable of perfectly fitting randomly labeled data. Recent evidence suggests that developing compressible representations is key for adjusting the complexity of overparametrized networks to the task at hand [4, 42]. In this paper, we provide new empirical evidence that supports this hypothesis by identifying two types of units that emerge when the network’s width is increased: removable units which can be dropped out of the network without significant change to the output and repeated units whose activities are highly correlated with other units. The emergence of these units implies capacity constraints as the function the network represents could be expressed by a smaller network without these units. In a series of experiments with AlexNet, ResNet and Inception networks in the CIFAR-10 and ImageNet datasets, and also using shallow networks with synthetic data, we show that DNNs consistently increase either the number of removable units, repeated units, or both at greater widths for a comprehensive set of hyperparameters. These results suggest that the mechanisms by which networks in the deep learning regime adjust their complexity operate at the unit level and highlight the need for additional research into what drives the emergence of such units.

1. Introduction

Deep neural networks (DNNs) are capable of successfully learning from examples in a wide variety of tasks. Though these networks are typically trained with large amounts of data, the number of free parameters in their architectures is

often several orders of magnitude greater than the number of training examples. This overparametrization reflects the ability of DNNs to memorize entire datasets, even with randomized labels [40]. Several previous studies have aimed to uncover why, out of the many optima an overparametrized network can reach to achieve 100% training accuracy, they tend toward ones that generalize well [28, 31, 41] often by proving generalization bounds related to weight matrix norms or Rademacher complexity [4, 6, 29].

A further striking feature of DNNs is that the test accuracies of wider, more overparametrized networks tend to be the same or better than thinner versions of themselves [9, 28, 30, 31, 32]. Although such wide models are strictly more expressive than their thinner counterparts, they nonetheless tend to avoid relative overfitting. While these DNNs appear to adapt their effective capacity to the complexity of the given task, precisely what causes them to do so remains an open question.

Frankle and Carbin [9] show that in certain DNNs, the crucial computations are performed by independent subnetworks with initializations primed for the learning task, *i.e.* such subnetworks have won the “initialization lottery”. In doing so, they suggest that wide networks may perform as well as or better than thin ones because they “buy more lottery tickets” and more reliably contain these fortuitously initialized subnetworks. However, regarding subnetworks that are not part of a winning lottery ticket, it remains unclear why they do not have a substantial effect on network output. Related to this question, recent theoretical work by Arora *et al.* [4] and Zhou *et al.* [42] builds from the observation that networks can often be compressed to thinner versions of themselves with little change in performance. They demonstrate that stronger generalization bounds can be proven for compressed networks, suggesting a link between compressibility and non overfitting.

In this paper, we investigate the ways in which wider networks form compressible representations that allow for their accuracy not to decrease relative to thinner ones. Our findings reveal that two capacity-constraining mechanisms

* Both first authors contributed equally.

¹ Boston Children’s Hospital, Harvard Medical School, MA, USA

² BCS, Massachusetts Institute of Technology, MA, USA

³ DIBRIS, Università degli Studi di Genova, Italy

⁴ Neuroscience Graduate Program, University of California San Francisco, CA, USA

⁵ Center for Brains, Minds, and Machines (CBMM)

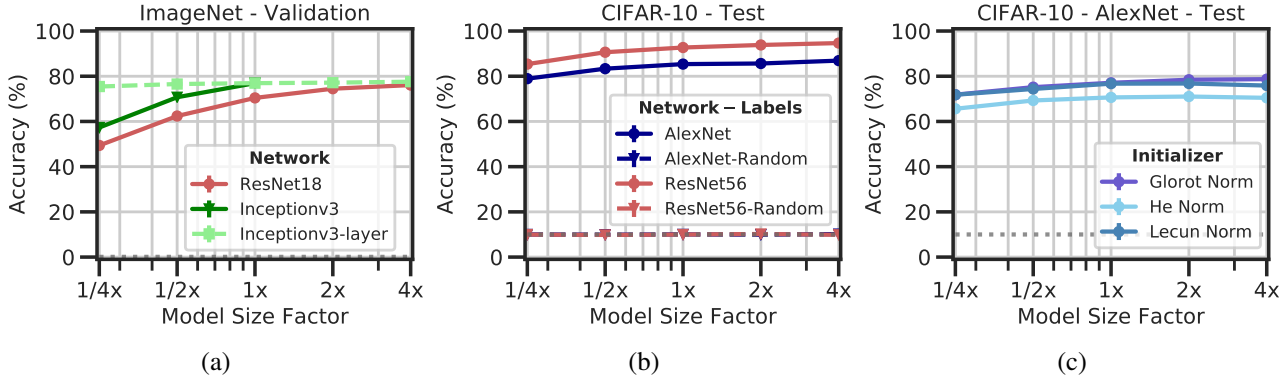


Figure 1: **Classification accuracy does not deteriorate with model size factor.** Top-1 test accuracies achieved across model sizes and datasets. (a) ResNet18s, Inception-v3s, and Inception-v3s with a single layer varied trained in ImageNet. (b) Regularized AlexNets and ResNet56s with and without training on random labels in CIFAR-10. "Random" refers to networks trained on randomly labeled data. (c) Glorot, He, and LeCun-initialized AlexNets in CIFAR-10.

develop at the individual unit-level: *removable units* which can be dropped out of the network without significant change to the output, and *repeated units* whose activities are highly correlated with other units. Through a comprehensive set of experiments, we find that DNNs train toward regimes that develop removable and repeated units to different extents, but that at least one of the two consistently emerges as the network's width is increased. These results provide an empirical perspective into the ways in which trained DNNs constrain their effective capacity at the individual unit level.

2. Unit-Level Autoregularization

In this section, we introduce the hypothesis that removable and repeated units emerge in overparametrized DNNs as a means of adjusting network complexity to the given task. The goal of this hypothesis is to explain the phenomenon shown in Fig. 1. For a variety of commonly used networks trained in ImageNet and CIFAR-10 using standard learning paradigms from the literature (experimental details are provided in section 3), we vary the number of units in fully connected layers and kernels in convolutional layers by a size factor. Note that this varies network width but not depth. We train these networks from scratch, tuning hyperparameters for all size factors. Fig. 1, reports test accuracies and demonstrates the well-known phenomenon that adding more units to networks leads to the same or better test accuracy in all cases [9, 28, 30, 31].

It has been suggested that an increase in overparametrization without loss of generality relates to a network's effective capacity being adjusted to the task at hand [4, 42]. This leads us to ask: What features do overparametrized networks develop that prevent them from utilizing their entire capacity? To answer this question, we focus on two capacity-constraining features at the unit-level: removable units and

repeated units.

2.1. Removable Units

A variety of network compression algorithms based on pruning nonessential units have been developed *e.g.* [13, 14, 17, 26]. The fact that DNNs can function well even when certain units are removed implies that not all units are necessary for effective performance. If a unit can be removed from a network without altering the network's output, it may as well not exist. If so, this would indicate that the network does not leverage its full capacity. In the following, we introduce removability from a theoretical point of view and how we can detect it in practice.

Removable Units in Theory. Let θ be a vector containing all the parameters of a DNN, *i.e.* all the weights. Also let \mathbf{x} be an input example and $f_{\theta}(\mathbf{x})$ be the mapping from the DNN input to its label. Let θ' be the parameters of the DNN with one or more units removed. If $f_{\theta}(\mathbf{x})$ is equal to $f_{\theta'}(\mathbf{x})$, the zeroed-out units are perfectly removable in the sense that they have no effect on the DNN and do not add to its complexity. This phenomenon could happen for multiple possible reasons ranging from simple explanations such as a unit never being activated or its outgoing weights all equaling 0, to more complex ones such as having the subsequent layers discard the activity of the unit. Additionally, due to interactions between the effects of multiple units, a set of units can be jointly removable without each member of the set being individually removable or vice versa. Further analysis of these possible mechanisms in future works may provide more detailed insights about how DNNs adjust their complexity.

Detecting Removable Units in Practice. Empirically evaluating how similar $f_{\theta}(\mathbf{x})$ and $f_{\theta'}(\mathbf{x})$ are is impossible in practice because only a finite number of samples can be obtained. Thus, we approximate the DNN function by evalu-

ating it on a testing set. We measure the proportion of images in the test set whose output labels remain unchanged after an ablation, referring to this as the *proportion of unchanged labels*.

Unfortunately, finding combinations of units that yield a certain proportion of unchanged labels is NP-hard. Because of this and the fact that a single unit may contribute differently to network output depending on the set of units that are ablated due to interactions between units, we do not directly evaluate whether each unit is individually removable or not. Instead, to investigate how removable on average the units across a network are in a computationally tractable way, we measure what proportion of labels do not change when random dropouts are applied to a certain proportion of units during evaluation. This process provides a general measure of how removable the units in a network are on average.

Fig. 2 provides examples of how resistant networks of two types are to unit ablation across different width factors. The testing accuracies of these networks are displayed in Fig. 1c. In all of the networks shown in Fig. 2, as more units are removed, more output labels change, showing that larger ablations produce larger deviations in the function represented by a network. Fig. 2a shows a case in which the labels output by wider networks are more resistant to the ablation of a given proportion of units than thinner networks. This implies that here, much of the wider networks’ excess capacity is being used for the development of removable units.

However, Fig. 2b shows a case in which resistance to the ablation of a proportion of units does not necessarily increase with model width in a set of networks that only differ from those in Fig. 2a by how they were initialized. This example demonstrates that removable units are not sufficient to explain the capacity constraints developed by DNNs at large sizes. This motivates the search for a second mechanism by which capacity constraints can be understood on the unit level.

2.2. Repeated Units

In contrast to compression approaches based on unit-pruning, other compression algorithms have been developed which replace similarly-activated clusters of units with merged units, e.g. [12, 35, 38]. These show that clusters of similarly-activated units may imply that a DNN is not leveraging its full capacity because they can be replaced by a smaller number of units without significantly altering network performance. In this sense, if two units are strongly correlated, we consider them to be *repeated*. In the following, we first discuss repeated units from a theoretical point of view, and then detail how we detect the degree to which units in a network are repeated in practice.

Repeated Units in Theory. Let \mathbf{w} be the incoming weights for a unit and let \mathbf{u} be the activations of the units in the

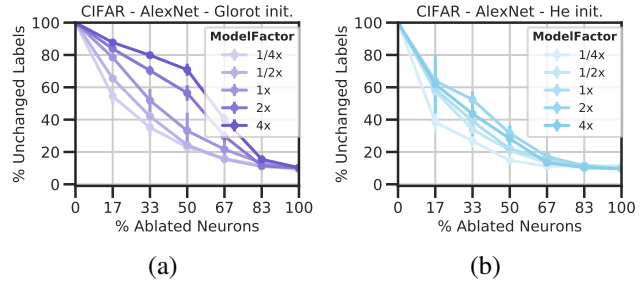


Figure 2: **Some networks develop more resistance to unit removal as model size increases.** Each point shows the proportion of labels that did not change when the percentage of units on the x-axis were randomly ablated. Networks were identically trained except for initialization and model size. (a) Glorot-initialized AlexNets in CIFAR-10. (b) He-initialized AlexNets in CIFAR-10.

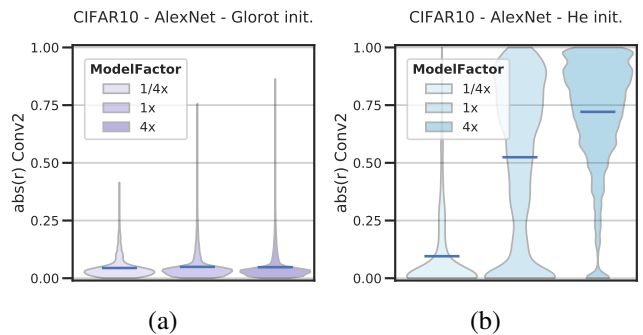


Figure 3: **Some networks develop more highly correlated units as model size increases.** Each violin plot shows the distribution of pairwise correlation coefficients for the final convolutional layer of the network across the testing set. Networks were identically trained except for initialization and model size. (a) Glorot-initialized AlexNets in CIFAR-10. (b) He-initialized AlexNets in CIFAR-10.

previous layer. Given the nonlinear activation function σ , $\sigma(\mathbf{w}^T \mathbf{u})$ is equal to the output activity of the unit. If two or more units in the previous layer have perfectly correlated activities, e.g. if \mathbf{u}_i is always equal to $\gamma \mathbf{u}_j$ for some constant γ , then it exists an equivalent smaller network without the repeated units. To show this, let \mathbf{w}' and \mathbf{u}' be the vector of incoming weights and activations, respectively, for a network in which \mathbf{u}_j has been removed. It is easy to see that if $\mathbf{w}'_i = \mathbf{w}_i + \gamma \mathbf{w}_j$, then $\sigma(\mathbf{w}^T \mathbf{u}) = \sigma(\mathbf{w}'^T \mathbf{u}')$ and hence, the network is not affected by the removal of \mathbf{u}_j . This shows that if the activities of one or more units are perfectly correlated, there is a functionally equivalent network with these redundant units taken out. Importantly, this contrasts with the way in which removable units as previously described can be taken from a network because cleanly taking a re-

peated unit out of a network may require adjusting network weights. To see examples of cases in which a repeated unit is and is not removable without making weight adjustments, see subsection 2.3.

Detecting Repeated Units in Practice. Perfect correlation between units cannot be expected to appear in practice. In order to scalably quantify the extent to which units in a DNN are repetitive, we analyze the distribution of all absolute valued pairwise Pearson correlation coefficients for the units in a network.

Fig. 3 shows examples giving the distributions of these coefficients for the final convolutional layers in networks of two types (differing only by initialization) whose testing accuracies are displayed in Fig. 1c. Fig. 3a shows a case in which the level of unit-to-unit correlation increases only very slightly as network width is increased. However, Fig. 3b shows a case in which much more unit-to-unit correlation develops with wider networks. This implies that here, excess capacity is largely being utilized for forming these highly correlated units.

2.3. Relating Removable and Repeated Units

Why this discrepancy between networks whose capacity constraints can be understood in terms of removable units and ones whose capacity constraints can be understood in terms of repeated units? Here, we clarify that these two mechanisms can emerge either together or independent of one another.

Let \mathcal{S} and \mathcal{L} denote respectively a narrow and a wide deep network with the same architecture. Let \mathbf{u} refer to the activity of the layer before the output layer in \mathcal{S} and \mathbf{w} the incoming weights of the output layer of \mathcal{S} . Thus, the output of \mathcal{S} is equal to $\mathbf{w}^T \mathbf{u}$. We now construct examples of a large network \mathcal{L} , twice the size of \mathcal{S} , that compute the same function as \mathcal{S} yet develop different amounts of removable and repeated units. There are many other possible cases than the ones presented here.

More of Both Removable and Repeated Units. We first introduce the case in which both mechanisms emerge together as a network’s size doubles. Observe that we can build an \mathcal{L} that has the same accuracy as \mathcal{S} by duplicating \mathcal{S} such that the layer before the output is $[\mathbf{u}, \mathbf{u}]$ and the output weights are equal to $[\mathbf{w}, \mathbf{0}]$. Because $[\mathbf{w}, \mathbf{0}]^T [\mathbf{u}, \mathbf{u}] = \mathbf{w}^T \mathbf{u}$, the outputs will be identical. In this scenario, both removable and repeated units would be greater in quantity in \mathcal{L} compared to \mathcal{S} , because half of the network is removable and repeated as the units for which weights are 0 are repeated and can be removed without affecting the network (they are multiplied by 0). Another example would be that \mathcal{L} is composed by \mathcal{S} and by units whose activity is always equal to 0, *i.e.* $[\mathbf{u}, 0]$, because such unresponsive units are removable and repeated.

Only More Removable Units. A case in which there are more removable units but not more repeated units can be

constructed by making the units before the output layer in \mathcal{L} equal to $[\mathbf{u}, \mathbf{v}]$, where \mathbf{v} are units with activities uncorrelated to \mathbf{u} and each other. Thus, the units are not repeated. To make \mathcal{L} compute the same function as \mathcal{S} , the weights of this network can be made equal to $[\mathbf{w}, \mathbf{0}]$, and as in the previous case, the units that are multiplied by 0 (half of the layer) are removable.

Only More Repeated Units. Finally, we can show a case in which there are more repeated units but not more removable units. Let the layer before the output in \mathcal{L} equal $[\mathbf{u}, \mathbf{u}]$, making half of the units repeated. We can obtain a network with the same accuracy as \mathcal{S} with the following weights leading into the output layer $[\frac{\mathbf{w}}{2} + \eta, \frac{\mathbf{w}}{2} - \eta]$, where η is a large constant. Although $[\frac{\mathbf{w}}{2} + \eta, \frac{\mathbf{w}}{2} - \eta]^T [\mathbf{u}, \mathbf{u}] = \mathbf{w}^T \mathbf{u}$, when a unit is removed, the output changes by an offset equal to $(\eta - \frac{w_k}{2})u_k$, where u_k is the removed unit, making the unit not removable when η is sufficiently large to change the output label.

2.4. The Unit-Level Autoregularization Hypothesis

Although neither the emergence of removable units nor repeated units alone are sufficient to explain how overparametrized networks constrain their capacity in Fig. 2 and 3, one might ask whether they are sufficient together. Section 4 provides evidence that they indeed are in practice. Consider a small deep network \mathcal{S} and a large one \mathcal{L} , both with the same architecture, trained on the same task with the same explicit regularization scheme and random initialization scheme, each with a tuned set of hyperparameters. Our hypothesis is that alongside \mathcal{L} generalizing as well or better than \mathcal{S} , \mathcal{L} will develop capacity constraining features that cause it to have more removable units and/or more repeated units than \mathcal{S} due to the effects of autoregularization. Note that this hypothesis is falsifiable through finding deep networks in which neither resistance to random ablation nor unit-correlation emerge with size. It is also falsifiable by showing cases in which removability or repetition were decoupled from our methods of measuring them. We hope that future work extending or challenging this hypothesis will lead to a richer understanding of the emergent properties of DNNs.

3. Experimental Setup

Table 1 gives training details for the networks we use. Features that we tested multiple variants of are marked with a star (*). Further details for all networks can be found in the Appendix. To see how unit removability and repetition vary as functions of a model’s degree of overparametrization, we tested variants of each network in which the number of weights/kernels in each layer/block/module were multiplied by factors of 1/4, 1/2, 1, 2, and 4.

Networks. For experiments with synthetic, uncorrelated data, we used simple multilayer perceptrons (MLPs) with 1

Dataset	Network	Initialization	Optimizer	Regularizers	L.Rate-B.Size
Uncorr. 10 dim	MLP	Normal*	Momentum	None	Best
Uncorr. 10k dim	MLP	Normal*	Momentum, SGD Adam *	None	Best
CIFAR-10 (+ rand. labels*)	AlexNet	Glorot/LeCun/He*	Momentum	None, DA, DO, WD*	Best*
	ResNet56	Glorot	Momentum	BN, DA, WD	Best*
ImageNet	ResNet18	Glorot	Momentum	BN, DA, WD	Best*
	Inception-v3	Normal	RMSProp	BN, DA, WD	Best

Table 1: **Network training and performance details:** “BN” refers to batch normalization, “DA” refers to data augmentation, “DO” refers to dropout, and “WD” refers to L2 weight decay. “Best” refers to learning rate/batch size combinations that we found to achieve the highest accuracy. Stars (*) indicate factors for which we tested multiple hyperparameters/variants.

hidden layer of 128 units for the 1x model size and ReLU activations. For experiments using CIFAR-10, we used scaled-down AlexNet models with two convolutional and two fully-connected layers based on Zhang et al. [40] and ResNet56s with initial convolutions and 3 block layers based on He et al. [16]. For the ImageNet dataset, we used ResNet18s with 4 block layers also based on He et al. [16] as well as Inception-v3 networks based on Szegedy et al. [36]. Fig. 1 shows the testing accuracy achieved by several of the ImageNet and CIFAR-10 networks. For these and all others tested, increasing model size results in either equal or improved performance. Due to hardware restrictions (we used a dgx1 with 8x NVIDIA V100 GPUs 32GB), we were not able to train any 2x or 4x sized Inception-v3s and instead experimented with versions of these networks where a single layer’s size varied from 1/4x to 4x (denoted as *Inceptionv3-layer* in plots). In the Appendix we plot the number of trainable parameters for each network, showing that they increase exponentially with model size.

Datasets. We used the ImageNet dataset [34] with approximately 1 million training images and 50,000 images for validation and the CIFAR-10 dataset [21] with a 45,000/5,000/10,000 train/validation/test split for the larger-scale experiments. For small-scale ones using MLPs, we used synthetic, uncorrelated data generated by randomly-initialized teacher MLPs with binary output identical in architecture to the 1/4x MLP models. The teacher networks output each label for between 40% and 60% of random inputs. We trained and evaluated the MLPs by default on datasets of 1,000 examples.

Initializations. By default, we initialized the MLP and Inception-v3 networks using normal distributions with mean 0 and a fixed σ^2 . In the MLPs, we experimented with various values for σ^2 . For the AlexNet and ResNet models, we defaulted to using normal Glorot initialization with mean 0 and variance, $\sigma^2 = 2/(fan_{in} + fan_{out})$ [11]. In the AlexNets, we also experiment with LeCun initialization for which $\sigma^2 = 1/fan_{in}$ [23], and He initialization, for which $\sigma^2 = 2/fan_{in}$ [15], as well as uniform initialization dis-

tributions of these three types.

Optimizers. We use RMSProp [37] in the Inception-v3s and the momentum optimizer in all other models by default. We also experiment with using momentumless stochastic gradient descent (SGD) and Adam [19] with the MLPs.

Stopping Criterion. All networks were trained for a fixed number of iterations except for the CIFAR-10 AlexNets which were trained to the epoch of maximum validation accuracy. In the Appendix, we show that the trends in these networks are invariant to the amount of training time after convergence in the ResNet18s, and we observe the same for all other models.

Regularizers. We train MLPs and AlexNets by default with no explicit regularization (except for early stopping in the AlexNets). We train all ResNets and the Inception-v3 networks with batch normalization, data augmentation, and weight decay. To test how explicit regularization contributes to unit removability and repetition, we also analyze AlexNets trained with data augmentation, dropout, weight decay, and all three combined.

Learning rates and Batch Sizes. Typically in DNNs, varying batch size and learning rate jointly by a constant factor tends to affect training time but not performance [20], and they are commonly varied in practice. To investigate its effects, we experiment with varying learning rate and batch size jointly by factors of 1/4, 1, and 4.

Evaluation of Unit-level Autoregularization. We use the procedures introduced in the previous section to evaluate the degree of removable and repeated units in the network. We measure removability and repetition using the following methods:

-Removable Units: We obtain ablation curves by dropping out units in fully connected layers and individual applications of convolutional kernels (which can be thought of as removing individual “units” of convolutional kernels). We calculate an ablation curve for every layer independently and average them in the displayed results. An example was shown in Fig. 2. In the following, we report the Area Under the Curve (AUC) of the ablation curve to summarize the

curve with a single number. High *AUC* values (the maximum possible is 1) indicate a high index of removable units.

-Repeated Units: We evaluate the extent to which a network forms repetitive units by calculating the absolute valued Pearson correlation between the activity of all pairs of units within a layer. The distribution of these pairwise comparisons was previously displayed in Fig. 3. We summarize the distribution with the average number of units for which the absolute valued correlation exceeds a certain threshold per unit. We refer to this as *similarity*. We calculate this for all layers and report the average across layers. In our plots, we use a relatively low threshold of 0.5 because it allows us to visualize trends in similarity even for networks such as the ones displayed in Fig. 3 in which it increases very little with width.

Samplings and Replicates. Due to the number of units in the models and the size of the datasets, analyzing all activation vectors for convolutional filters was intractable. Instead, we based our measures on a sampling of units capped at 50,000 per layer. We average across three independent samplings and find that the variance between them is negligible for all networks. For each model, we also average across layers, except for the Inceptionv3-layer curves which are only for the layer whose size is varied. We also average results across three independently-trained model replicates, except for the ResNet18s and Inception-v3s. All error bars for *AUC* plots show standard deviation between independently trained model replicates when applicable and independent samplings of units when not. They are typically too small to appear in plots. Error bars for similarity plots show average standard deviation within trials. For all experiments, we display only results for the test/validation set because results from the train set (except for accuracy) were almost identical.

4. Results

Here, we present our findings for how removability and repetition vary as a function of model size. We experiment across a wide variety of networks, hyperparameters, and training methods used in modern deep learning research. Removability and/or repetition emerge as model size increases for all deep networks tested.

Removability emerges and repetition varies in ImageNet models. Fig. 4 shows that the ResNet18 and Inception-v3 models both become more resistant to ablation as their model sizes increase, conforming to the hypothesis. They also demonstrate the independence of removability and repetition with the ResNet18s developing more repeated units and the Inception-v3s losing them with size.

Removability and repetition develop in networks trained on randomly-labeled data. Our central question revolves around how DNNs are able to constrain their effective capacity to the task at hand, so it is natural to study removability and repetition in non-generalizing networks

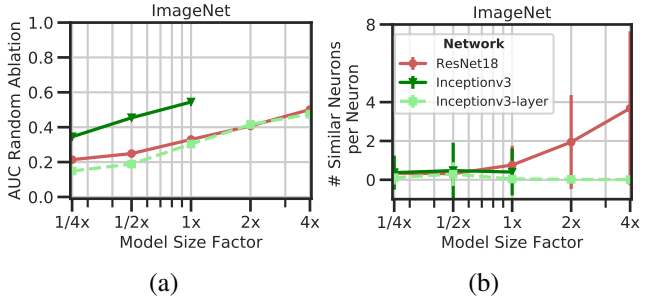


Figure 4: **Unit removability and repetition emerge in ResNet18s, removability alone in Inception-v3s (ImageNet).** (a) Areas under random ablation curves, (b) the average number of similar units per unit. Each point is an average across layers except for the points in the Inceptionv3-layer curves which are only for that layer.

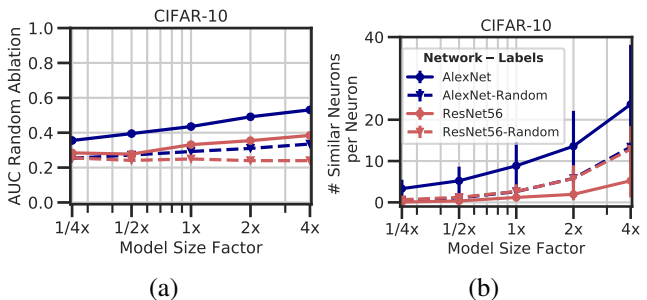


Figure 5: **Unit removability and/or repetition emerge in AlexNet and ResNet56 models, even when trained on randomly labeled data (CIFAR-10).** (a) Areas under ablation curves, (b) the average number of similar units per unit. Each point is an average across layers.

trained to memorize randomly labeled images. Fig. 5 compares the results with AlexNet and ResNet56 models trained on both uncorrupted and randomly-labeled CIFAR-10. With random labels, all networks of the 1x size or greater were able to fit the training set with perfect or near-perfect performance. Even when fitting randomly labeled data, these models follow our central hypothesis, developing significant levels of unit removability and/or repetition at large sizes. Curiously, in the ResNet56 models, fitting random labels causes removability to flatline but repetition to increase relative to the models trained on correctly-labeled data. This strongly indicates that although removability and repetition imply capacity constraint, they do not imply generalization, nor does generalization imply them.

Removability and repetition are sensitive to weight initialization. Some recent work has suggested that network initialization has a large influence over generalization behavior [8, 9, 39]. To see what effects it may have on removability and repetition, we test several common methods of

weight initialization. Fig. 6 presents results for AlexNets trained with Glorot, He, and Lecun initializations which initialize weights using normal distributions with variances of $2/(fan_{in} + fan_{out})$, $2/fan_{in}$, and $1/fan_{in}$ respectively. Removability increases with model size for the Glorot and Lecun-initialized nets but exhibits a fairly flat trend for the He-initialized nets, which demonstrate a case where removability does not emerge at large sizes. Meanwhile, for the Lecun and He-initialized nets, some model size factor doublings coincide with more than a doubling of the number of similar units per unit, perhaps reflecting a fairly sharp transition to a differently-behaving regime when initialization variance becomes high enough. We also test AlexNets with uniform Glorot, He, and LeCun initializations and find their results to be very similar to those of the networks with normally distributed initial weights (see Appendix), suggesting that the initialization distribution matters little compared to the initialization variance.

The dimensionality of input data may drive the emergence of removability and repetition. Adding to our analysis of initializations, in the Appendix we show the results of altering initialization variance in MLPs trained on uncorrelated data. Those initialized with small variance develop more repeated units at larger model sizes. However, we find that the MLPs initialized with very high variance develop neither more removability nor repetition. Note this is not the case for similar MLPs trained on low dimensional data, suggesting that this phenomenon in which neither removability nor repetition increases is related to high dimensionality in data. This case with a single layer MLP, high initialization, and high dimensional, uncorrelated data demonstrates one case in which neither removability nor repetition emerges. This suggests that input data may play a critical role in driving the emergence of removable and/or repeated units.

Our hypothesis holds under a number of additional tests. In the Appendix we present a number of experiments which further support the unit-level autoregularization hypothesis.

While individual layers in the ResNets and Inception-v3s display unique trends, each develops more removability or unit-repetition at higher sizes and generally follows the trend of its network as a whole. We find no consistent relationship between a layer’s depth and how removable or repeated its units are.

Because we hypothesize that removability and repetition in DNNs is a result of autoregularization, we explore their trends in networks trained with and without explicit regularization. In the Appendix, we show that data augmentation, dropout, weight decay, and all three together can change the amount of removability and repetition developed in the CIFAR-10 AlexNet models, but not the overall trends.

To investigate the influence of optimizers, we test training the MLP models using stochastic gradient descent (SGD), momentum, and Adam. The results (see Appendix) shows

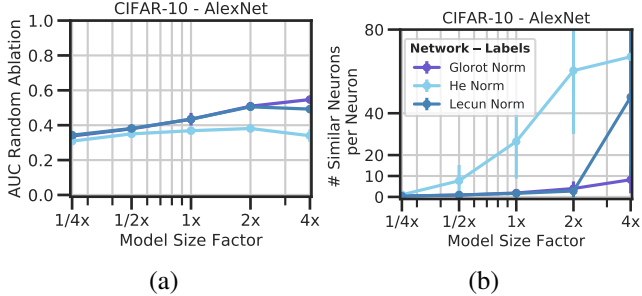


Figure 6: **Initialization influences unit removability and repetition.** Glorot initialization leads to repetition without replication, He initialization leads to repetition without removability, and LeCun initialization leads to intermediate results in AlexNets (CIFAR-10) (a) Areas under ablation curves, (b) the average number of similar units per unit. Each point is an average across layers.

that varying these optimizers can affect how much removability and repetition develop, but they do not change overall trends. Additionally, to see if removability and repetition depend on learning rate and batch size, we test the ResNet18, ResNet56, and AlexNet models trained on ImageNet and CIFAR-10 with several experiments in which we vary learning rate and batch size while keeping them proportional. Results in the Appendix show that this has little to no effect on outcomes.

5. Related Work and Discussion

In this work, we analyze how resistant networks are to unit removal and how correlated the activations of their units are as a means of understanding what types of capacity constraining features large networks develop. We scale our analysis to state of the art networks including AlexNets, ResNets, and Inception-v3s, showing that removability and/or repetition of units consistently increase alongside network width. By focusing not on the broad question of why networks generalize, but on the subproblem of why their testing accuracy does not tend to decrease when their width is increased, we provide evidence that removability and repetition are central to how networks autoregularize.

Despite a great deal of recent progress, to our knowledge, ours is the first work to date that has quantitatively studied the connections between overparametrization, removability, and repetition together. We analyze these phenomena across a wide range of networks which may aid in understanding how well theoretical findings (which are typically based on simple models) generalize to key settings in modern machine learning. Each DNN that we analyze displays unique trends in removability and repetition yet that one of the two increases alongside model width in all deep networks tested. We demonstrate that the two are highly dependent on weight

initializations and may be driven in part by the dimensionality of input data. Finally, we show that these units do not imply generalization.

Relations to works involving network compression. A related branch of work has focused on the relationship between a network’s compressibility and its generalization behavior [4, 42], and other work suggests that DNNs preferably learn simple representations over complex ones [2, 3, 5, 10, 27]. Network compression approaches based on pruning unimportant units or weights [1, 9, 14, 17, 24, 33] have suggested that the crucial computations within overparametrized networks only tend to be performed by relatively small subnetworks. Meanwhile, correlation-based compression methods which prune or merge highly correlated units have also been successful [12, 35, 38]. Our results generally validate compression approaches based on compressing both removable or repeated units, but we show that different networks develop different compressible features and to different extents, suggesting that combinations of various methods may be complementary tools for developing new compression algorithms. We also find that unit correlation is highly sensitive to a network’s initialization. This suggests that some compression techniques might be able to be improved by validating over multiple network initializations in order to produce models with a maximal degree of unit-to-unit correlation. We also make progress toward tightening our understanding of how compressible DNNs are which Zhou *et al.* [42] show can lead to improved generalization bounds.

Limitations and future directions. Limitations of this work include that we do not analyze how the removability and repetition of units vary with model depth. Also, more work is needed toward better characterizing specific types of capacity constraints that form in networks as well as the causal relationships between removability, repetition, and various factors of network training (especially initialization and input data). The fact that the single-layer MLPs with large initializations trained with high-dimensional, uncorrelated data do not seem to develop either increased removability or repetition at large model sizes poses a case which challenges our framework. However, a recent strand of research has emerged illuminating similarities between deep networks and kernel machines [7, 18, 25] and suggesting that networks with high-variance initializations can operate in a kernel-like regime [8, 39] which may relate to these findings for networks initialized with large variance.

6. Conclusion

In this paper, we analyzed the emergence of removable and repeated units in relation to the fact that the generalization ability does not tend to decrease as a network’s degree of overparametrization increases. In doing so, we found that the number of removable units and/or repeated units consistently increases alongside overparametrization. Observing these

units provides new evidence to support current theoretical results that propose compressing a trained network before measuring its complexity [4, 42], and also suggests that the capacity-constraining features which DNNs develop emerge at the individual unit level. We hope that these results will motivate future work investigating the processes that drive the emergence of capacity constraints in deep networks.

Acknowledgments

We are grateful to Tomaso Poggio for helpful feedback and discussions. This work is supported by the Center for Brains, Minds and Machines (funded by NSF STC award CCF-1231216), the Harvard office for Undergraduate Research and Fellowships, Fujitsu Laboratories (Contract No. 40008401) and the MIT-Sensetime Alliance on Artificial Intelligence.

References

- [1] Madhu S Advani and Andrew M Saxe. High-dimensional dynamics of generalization error in neural networks. *arXiv preprint arXiv:1710.03667*, 2017. 8
- [2] Jose M Alvarez and Mathieu Salzmann. Learning the number of neurons in deep networks. In *NIPS*, 2016. 8
- [3] Alessio Ansuini, Alessandro Laio, Jakob H Macke, and Davide Zoccolan. Intrinsic dimension of data representations in deep neural networks. *arXiv preprint arXiv:1905.12784*, 2019. 8
- [4] Sanjeev Arora, Rong Ge, Behnam Neyshabur, and Yi Zhang. Stronger generalization bounds for deep nets via a compression approach. In *ICML*, 2018. 1, 2, 8
- [5] Devansh Arpit, Stanisław Jastrzębski, Nicolas Ballas, David Krueger, Emmanuel Bengio, Maxinder S Kanwal, Tegan Maharaj, Asja Fischer, Aaron Courville, Yoshua Bengio, et al. A closer look at memorization in deep networks. In *ICML*, 2017. 8
- [6] Peter L Bartlett, Dylan J Foster, and Matus J Telgarsky. Spectrally-normalized margin bounds for neural networks. In *NIPS*, 2017. 1
- [7] Mikhail Belkin, Siyuan Ma, and Soumik Mandal. To understand deep learning we need to understand kernel learning. In *ICML*, 2018. 8
- [8] Lenaïc Chizat, Edouard Oyallon, and Francis Bach. On lazy training in differentiable programming. *arXiv preprint arXiv:1812.07956*. 6, 8
- [9] Jonathan Frankle and Michael Carbin. The lottery ticket hypothesis: Finding sparse, trainable neural networks. In *ICLR*, 2019. 1, 2, 6, 8
- [10] Gauthier Gidel, Francis Bach, and Simon Lacoste-Julien. Implicit regularization of discrete gradient dynamics in deep linear neural networks. In *NeurIPS*, 2019. 8
- [11] Xavier Glorot and Yoshua Bengio. Understanding the difficulty of training deep feedforward neural networks. In *AISTATS*, 2010. 5

- [12] Yunchao Gong, Liu Liu, Ming Yang, and Lubomir Bourdev. Compressing deep convolutional networks using vector quantization. *arXiv preprint arXiv:1412.6115*, 2014. 3, 8
- [13] Song Han, Huizi Mao, and William J Dally. Deep compression: Compressing deep neural networks with pruning, trained quantization and huffman coding. In *ICLR*, 2015. 2
- [14] Song Han, Jeff Pool, John Tran, and William Dally. Learning both weights and connections for efficient neural network. In *NIPS*, 2015. 2, 8
- [15] Kaiming He, Xiangyu Zhang, Shaoqing Ren, and Jian Sun. Delving deep into rectifiers: Surpassing human-level performance on imagenet classification. In *ICCV*, 2015. 5
- [16] Kaiming He, Xiangyu Zhang, Shaoqing Ren, and Jian Sun. Deep residual learning for image recognition. In *CVPR*, 2016. 5, 10
- [17] Hengyuan Hu, Rui Peng, Yu-Wing Tai, and Chi-Keung Tang. Network trimming: A data-driven neuron pruning approach towards efficient deep architectures. *arXiv preprint arXiv:1607.03250*, 2016. 2, 8
- [18] Arthur Jacot, Franck Gabriel, and Clément Hongler. Neural tangent kernel: Convergence and generalization in neural networks. In *NeurIPS*, 2018. 8
- [19] Diederik P Kingma and Jimmy Ba. Adam: A method for stochastic optimization. In *ICLR*, 2014. 5
- [20] Alex Krizhevsky. One weird trick for parallelizing convolutional neural networks. *arXiv preprint arXiv:1404.5997*, 2014. 5, 11
- [21] Alex Krizhevsky, Geoffrey Hinton, et al. Learning multiple layers of features from tiny images. Technical report, Citeseer, 2009. 5
- [22] Alex Krizhevsky, Ilya Sutskever, and Geoffrey E Hinton. Imagenet classification with deep convolutional neural networks. In *Advances in neural information processing systems*, pages 1097–1105, 2012. 10
- [23] Yann A LeCun, Léon Bottou, Genevieve B Orr, and Klaus-Robert Müller. Efficient backprop. In *Neural networks: Tricks of the trade*, pages 9–48. Springer, 2012. 5
- [24] Chunyuan Li, Heerad Farkhoor, Rosanne Liu, and Jason Yosinski. Measuring the Intrinsic Dimension of Objective Landscapes. In *ICLR*, 2018. 8
- [25] Tengyuan Liang and Alexander Rakhlin. Just interpolate: Kernel" ridgeless" regression can generalize. *Annals of Statistics*, 2019. 8
- [26] Jian-Hao Luo, Jianxin Wu, and Weiyao Lin. Thinet: A filter level pruning method for deep neural network compression. In *ICCV*, 2017. 2
- [27] Hartmut Maennel, Olivier Bousquet, and Sylvain Gelly. Gradient descent quantizes relu network features. *arXiv preprint arXiv:1803.08367*, 2018. 8
- [28] Behnam Neyshabur, Srinadh Bhojanapalli, David McAllester, and Nati Srebro. Exploring generalization in deep learning. In *NIPS*, 2017. 1, 2
- [29] Behnam Neyshabur, Srinadh Bhojanapalli, David McAllester, and Nathan Srebro. A pac-bayesian approach to spectrally-normalized margin bounds for neural networks. In *ICLR*, 2018. 1
- [30] Behnam Neyshabur, Zhiyuan Li, Srinadh Bhojanapalli, Yann LeCun, and Nathan Srebro. The role of over-parametrization in generalization of neural networks. In *ICLR*. 1, 2
- [31] Roman Novak, Yasaman Bahri, Daniel A Abolafia, Jeffrey Pennington, and Jascha Sohl-Dickstein. Sensitivity and Generalization in Neural Networks: an Empirical Study. In *ICLR*, 2018. 1, 2
- [32] Tomaso Poggio, Kenji Kawaguchi, Qianli Liao, Brando Miranda, Lorenzo Rosasco, Xavier Boix, Jack Hidary, and Hrushikesh Mhaskar. Theory of deep learning iii: explaining the non-overfitting puzzle. *arXiv preprint arXiv:1801.00173*, 2017. 1
- [33] Maithra Raghu, Ben Poole, Jon Kleinberg, Surya Ganguli, and Jascha Sohl-Dickstein. On the expressive power of deep neural networks. *PMLR*, 2017. 8
- [34] Olga Russakovsky, Jia Deng, Hao Su, Jonathan Krause, Sanjeev Satheesh, Sean Ma, Zhiheng Huang, Andrej Karpathy, Aditya Khosla, Michael Bernstein, Alexander C. Berg, and Li Fei-Fei. ImageNet Large Scale Visual Recognition Challenge. *IJCV*, 2015. 5
- [35] Suraj Srinivas and R Venkatesh Babu. Data-free parameter pruning for deep neural networks. In *BMVC*, 2015. 3, 8
- [36] Christian Szegedy, Vincent Vanhoucke, Sergey Ioffe, Jon Shlens, and Zbigniew Wojna. Rethinking the inception architecture for computer vision. In *CVPR*, 2016. 5, 10
- [37] T. Tieleman and G. Hinton. Lecture 6.5—RmsProp: Divide the gradient by a running average of its recent magnitude. COURSER, 2012. 5
- [38] Wenxiao Wang, Cong Fu, Jishun Guo, Deng Cai, and Xiaofei He. Cop: Customized deep model compression via regularized correlation-based filter-level pruning. In *IJCAI*, 2019. 3, 8
- [39] Blake Woodworth, Suriya Gunasekar, Jason Lee, Daniel Soudry, and Nathan Srebro. Kernel and deep regimes in overparametrized models. *arXiv preprint arXiv:1906.05827*, 2019. 6, 8
- [40] Chiyuan Zhang, Samy Bengio, Moritz Hardt, Benjamin Recht, and Oriol Vinyals. Understanding deep learning requires rethinking generalization. In *ICLR*, 2017. 1, 5, 10
- [41] Chiyuan Zhang, Qianli Liao, Alexander Rakhlin, Karthik Sridharan, Brando Miranda, Noah Golowich, and Tomaso Poggio. Theory of Deep Learning III: Generalization Properties of SGD. *CBMM Memo*, (067), 2017. 1
- [42] Wenda Zhou, Victor Veitch, Morgane Austern, Ryan P Adams, and Peter Orbanz. Non-vacuous generalization bounds at the imagenet scale: a pac-bayesian compression approach. In *ICLR*, 2019. 1, 2, 8

A. Experimental Details (Section 3)

A.1. Network Implementations

ResNet18s for ImageNet: We use the off-the-shelf models from [16]. They consisted of an initial convolution and batch norm followed by four building blocks (v1) layers, each with two blocks and a fully connected layer leading to a softmax output. All kernel sizes in the initial layers and block layers were of size 7×7 and stride 2. All activations were ReLU. In the 1x sized model, the convolutions in the initial and block layers used 64, 64, 128, and 256 filters respectively. We followed the standard training procedure. After Glorot initialization, we trained them for 90 epochs with a default batch size of 256 an initial default learning rate of 1 which decayed by a factor of 10 at epochs 30, 60, and 80. Optimization was done with SGD using 0.9 momentum. We used batch normalization, data augmentation with random cropping and flipping, and 0.0001 weight decay.

Inception-v3s for ImageNet: We used the off-the-shelf models from [36]. For the sake of brevity, we will omit architectural details here. We followed the standard training procedure. After using a truncated normal initialization with $\sigma = 0.1$, we trained them for 90 epochs with a default batch size of 256 and initial default learning rate of 1 with an exponential decay of 4% every 8 epochs. Training was done for 90 epochs on ImageNet. Optimization was done with the RMSProp optimizer. We used a weight decay of 0.00004, augmentation with random cropping and flipping, and batch norm with 0.9997 decay on the mean and an epsilon of 0.001 to avoid dividing by zero. Due to hardware constraints, we were not able to train 2x and 4x variants of the network (we used a dgx1 with 8x NVIDIA V100 GPUs 32GB). Instead, we trained the 1/4x-1x sizes along with versions of the network with 1/4x-4x sizes for a the "mixed 2: 35 x 35 x 288" layer only.

AlexNet for CIFAR-10: We use a scaled-down version of the network developed by [22] similar to the one used by [40] for CIFAR-10. The network consisted of a 5-layers: two convolutional layers and three dense layers. In each convolutional layer, 5×5 filters with stride 1 were applied, followed by max-pooling with a 3×3 kernel and stride 2. Local response normalization with a radius of 2, $\alpha = 2 * 10^{-05}$, $\beta = 0.75$ and $\text{bias} = 1.0$ was applied after each pooling. Each layer contained bias terms, and all activations were ReLU. In the 1x sized model, the convolutions used 96 and 256 filters, while the dense layers used 384, and 192 units. We trained these networks with early stopping based on maximum performance on a 5,000 image validation set. Weights were optimized with SGD using 0.9 momentum with an initial learning rate of 0.01, exponentially decaying by 5% every epoch. By default, and unless otherwise stated, we used Glorot initialization, a batch size of 128, and no explicit regularizers.

ResNet56s for CIFAR-10: These networks were off-the-shelf models by [16]. They consisted of an initial convolution and batch norm followed by three building block (v1) layers, each with nine blocks, and a fully connected layer leading to a softmax output. Kernels in the initial layers and block layers were of size 3×3 and stride 1. All activations were ReLU. In the 1x sized model, the convolutions in the initial and block layers used 16, 16, 32, 64, and 128 filters respectively. After initializing with Glorot initialization, we trained them for 182 epochs with a default batch size of 128 and an initial default learning rate of 1 which decayed by a factor of 10 at epochs 91 and 136. Optimization was done with SGD using 0.9 momentum. We used batch normalization, data augmentation with random cropping and flipping (except for our variants trained on randomly labeled data), and 0.0002 weight decay.

MLPs: We use simple multilayer perceptrons with either 10 or 10,000 inputs and binary output. They contained a single hidden layer with 128 units for the 1x model sizes and a bias unit. All hidden units were ReLU activated. Weights were initialized using a normal distribution with default σ of 0.01. Each was trained by default for 50 epochs on 1,000 examples produced by a 1/4x sized teacher network with the same architecture which was verified to produce each output for between 40% and 60% of random inputs.

A.2. Number of Parameters

In Fig. B1, we show the number of trainable parameters for each of our networks, showing that they increase exponentially with model size.

A.3. Stopping Criterion

In Fig. B2, we show that the trends of the removable and repeated unit evaluations are invariant to the amount of training time after convergence in the ResNet18s. We observe the same for all other models.

B. Additional Results (Section 4)

B.1. Removability and repetition are sensitive to weight initialization

We also test AlexNets with uniform Glorot, He, and Le-Cun initializations. Fig. B3 shows that their results are very similar to those of the networks with normally distributed initial weights, suggesting that the initialization distribution matters little compared to the initialization variance.

B.2. The dimensionality of input data may drive the emergence of removability and repetition

In Fig. B4 and B5, we show the results of altering initialization variance in MLPs trained on uncorrelated data. Those initialized with small variance develop more repeated units at larger model sizes. In Fig. B4, we can see that the MLPs

initialized with very high variance develop neither more removability nor repetition. However, this is not the case for similar MLPs trained on low dimensional data (Fig. B5), suggesting that this phenomenon in which neither removability nor repetition increases is related to high dimensionality in data.

B.3. The hypothesis holds under a number of additional tests

Per Layer Analysis. In Fig. B6, B7, B8 and B9, we show that while individual layers in our ResNets and Inception-v3s for CIFAR-10 and ImageNet display unique trends, each develops more removability or unit-repetition at higher sizes and generally follows the trend of its network as a whole. All layers display this trend, except for Inceptionv3-layer (Fig. B9), in which only the layer that we increase its width increases the removability while the other layers' removability remain constant.

Regularizers. In Fig. B10, we show results for AlexNet in CIFAR-10 with data augmentation, dropout, weight decay, and all three together. The regularizers increase the amount of removability and repetition developed in the models, but not the overall trends.

Optimizers. We test the effect of different optimizers in the MLP with the 10,000 dimensional dataset. In Fig. B11, we show that the optimizers affect how much removability and repetition develop, but they do not change overall trends.

Batch Size and Learning Rate. We vary a constant factor, which we denote as k , the batch size and the learning rate. This was found by [20] that it does not affect the performance but facilitates speeding up the convergence. In Fig. B12, we report the results for ResNet18 ImageNet and in Fig. B13 for ResNet56 and AlexNet in CIFAR-10. In all tested cases, the batch size and learning rate do not affect the trends of the removability and number of repeated units.

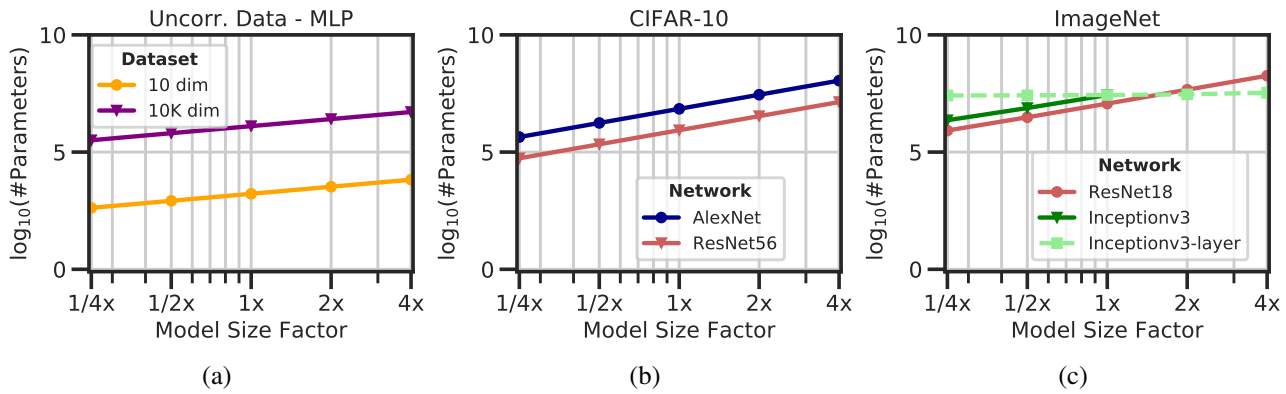


Figure B1: **Parameters**: (a) Multilayer perceptrons, (b) AlexNets and ResNet56s, (c) ResNet18s, Inception-v3s, and Inception-v3s with a single layer varied. The log number of trainable parameters at each model size.

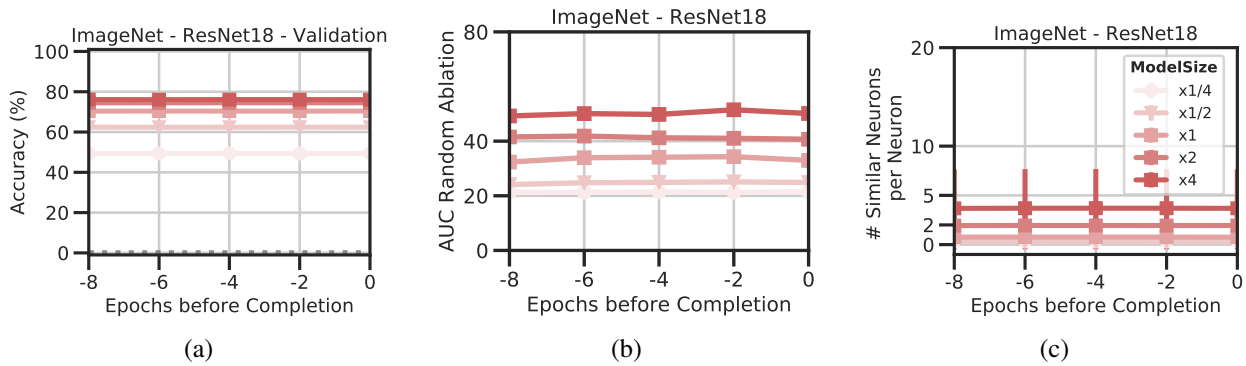


Figure B2: **Removability and repetition are invariant in ResNet18s under different amounts of training past convergence (ImageNet)**. Trends in (a) accuracy, (b) removability, and (c) similarity across training epochs after convergence in ResNet18.

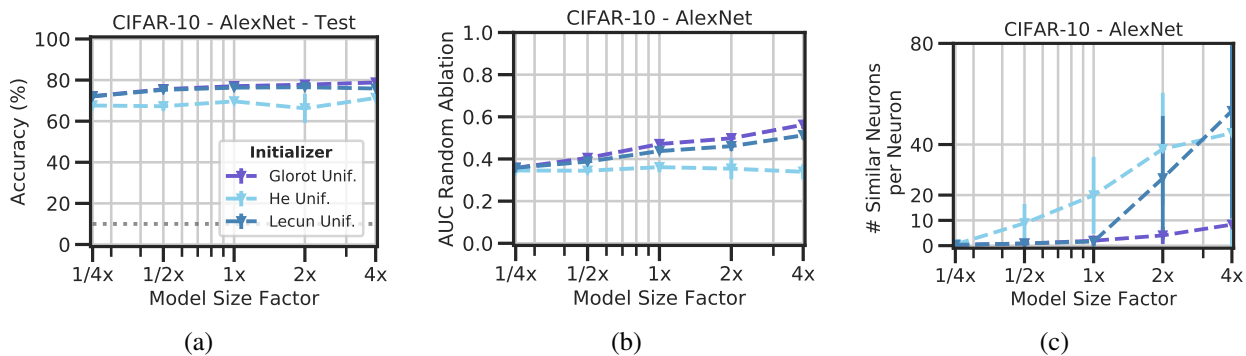


Figure B3: **AlexNet robustness and redundancy trends with uniform initializations resemble those with normal initializations (CIFAR-10)**. Trends in (a) accuracy, (b) removability, and (c) similarity with He, LeCun, and Glorot uniform initializations across size factors for AlexNets.

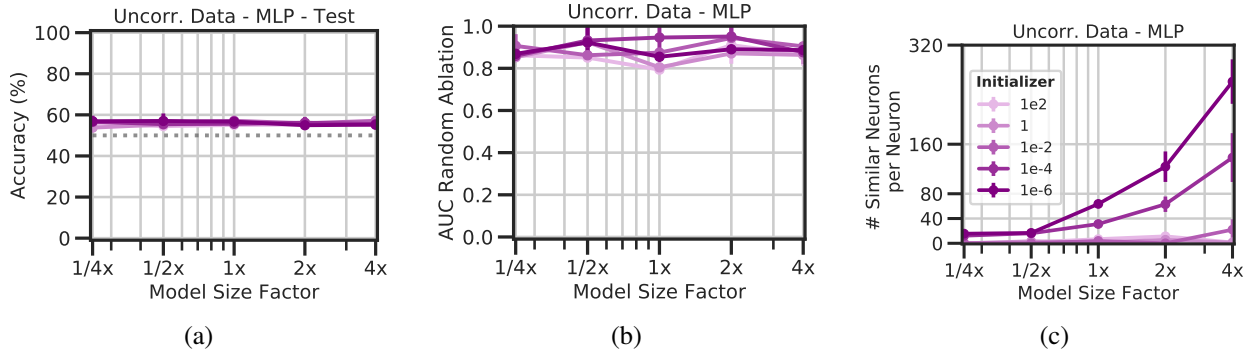


Figure B4: **The emergence of removability is sensitive to initialization variance in MLPs trained on 10,000 dimensional data.** Trends in (a) accuracy, (b) removability, and (c) similarity with multiple initialization variances across size factors for MLPs trained on 10,000 dimensional synthetic uncorrelated data. The legend gives σ for the normal weight initialization. Each initialization results in similar, flat accuracy and removability curves. Low variance initializations developed more similarity with size, but high variance did not.

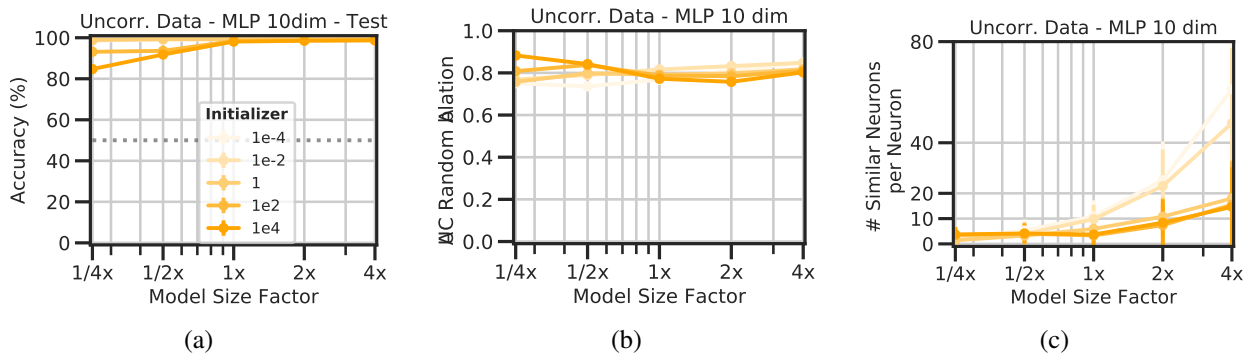


Figure B5: **The emergence of redundancy is not sensitive to initialization variance in MLPs trained on 10 dimensional data.** Trends in (a) accuracy, (b) robustness, and (c) similarity with multiple initialization variances across size factors for MLPs trained on 10,000 dimensional synthetic uncorrelated data. The legend gives σ for the normal weight initialization. Each initialization results in similar, flat accuracy and removability curves. All models developed more similarity with size.

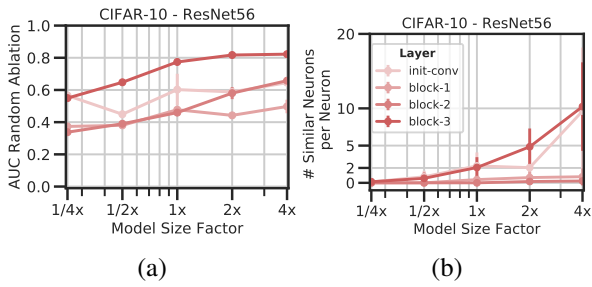


Figure B6: **ResNet56 robustness and redundancy layer-wise (CIFAR-10)**: Trends in (a) removability and (b) similarity among layers/blocks within ResNet56 in CIFAR-10. Each layer/block has a unique curve, with the initial convolutional and final block layers exhibiting the most removability and similarity.

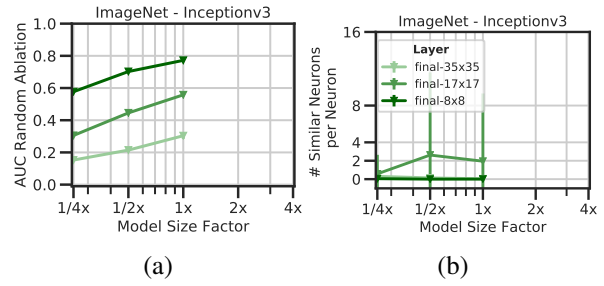


Figure B8: **Inception-v3 robustness and redundancy layer-wise (ImageNet)**: Trends in (a) removability and (b) similarity among the final 35×35 , 17×17 , and 8×8 blocks within Inception-v3 in ImageNet. Layers develop resistance to removal in order of their depth in the network, and the final 17×17 layer is the most similar.

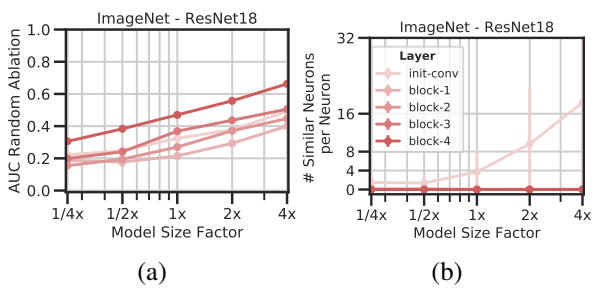


Figure B7: **ResNet18 robustness and redundancy layer-wise (ImageNet)**: Trends in (a) removability and (b) similarity among layers/blocks within ResNet18 in ImageNet. The final block layer is the most resistant to unit removal while the initial convolutional layer is the most similar.

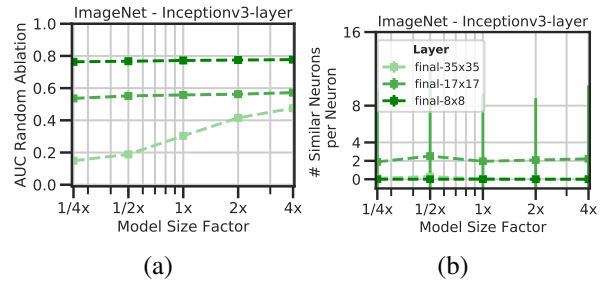


Figure B9: **Inception-v3 single layer robustness and redundancy layer-wise (ImageNet)**: Trends in (a) and (b) removability among the final 35×35 , 17×17 , and 8×8 blocks within Inception-v3s in ImageNet as only the final 35×35 layer is varied in size. Varying the size of a single layer has little or no effect on the unit removability and similarity of other layers.

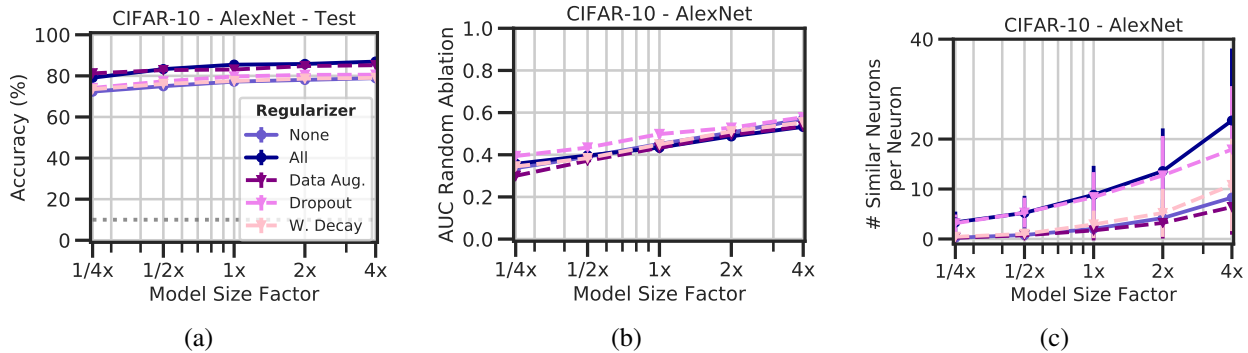


Figure B10: **Explicit regularization affects amounts but not trends for unit removability and similarity in AlexNets (CIFAR-10).** Trends in (a) accuracy, (b) removability, and (c) similarity with various explicit regularizers across size factors for AlexNets. We test data augmentation, dropout, weight decay, and all three together against the unregularized control. Each regularizer positively affects generalization performance, though weight decay only has a slightly positive effect. None serve to change the general trends in units removability and similarity, but they shift the curves up or down. Dropout and weight decay have a large and small positive effect on removability and similarity respectively. We attribute this to dropout forcing networks to develop redundant units to cope with ablations and weight decay pushing the weights of the network toward a smaller subspace.

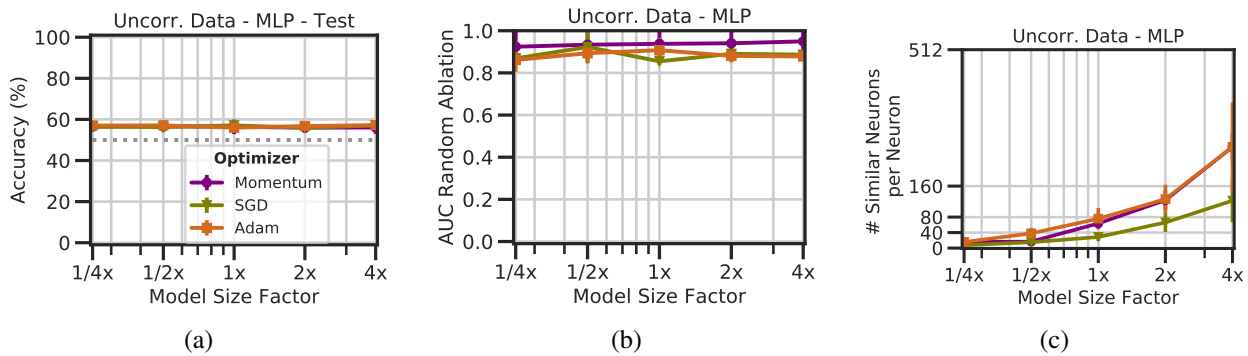


Figure B11: **Various optimizers result in different amounts but not different trends in unit removability and similarity in MLPs (Uncorrelated 10,000 dimensional synthetic data).** Trends in (a) accuracy, (b) robustness, and (c) similarity with momentum, stochastic gradient descent, and Adam optimizers across size factors for MLPs trained on 10,000 dimensional synthetic uncorrelated data. All three optimizers result in similar, flat curves in accuracy and removability but increases for similarity with size. Momentum and Adam result in more similarity than SGD.

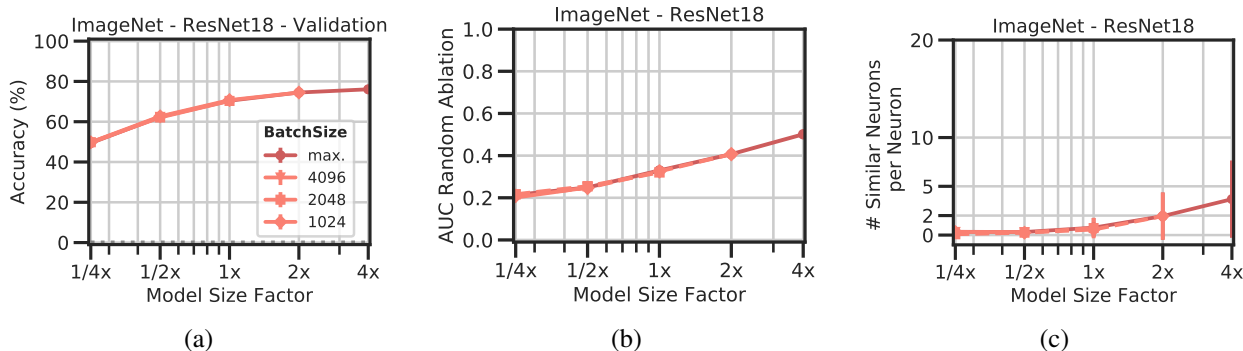


Figure B12: **Unit removability and similarity do not depend on learning rate and batch size factor in ResNet18 (ImageNet).** Trends in (a) accuracy, (b) removability, and (c) similarity across model sizes. We vary a constant factor k from 1/4 to 4 as a multiplier for the batch sizes and learning rates. “Max” refers to the maximum batch size that could be used for training a model given available hardware (dgx1 with 8x NVIDIA V100 GPUs 32GB).

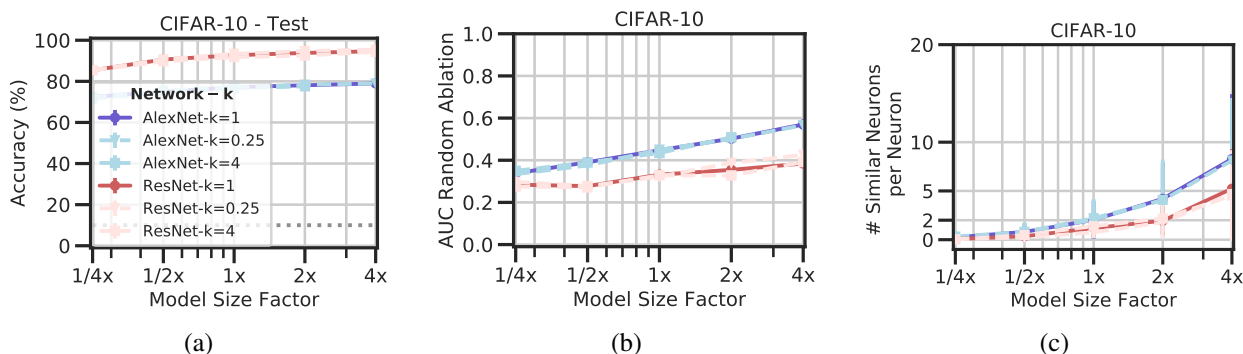


Figure B13: **The learning rate and batch size factor do not affect trends in unit removability and similarity in AlexNets and ResNet56s (CIFAR-10).** Trends in (a) accuracy, (b) removability, and (c) similarity across model sizes for AlexNets and ResNet56s. We vary a constant factor k from 1/4 to 4 as a multiplier for the batch sizes and learning rates. 4x AlexNets with $k = 4$ were not trained due to hardware restrictions. Compressibility tends to be slightly higher with higher k .